Journal of King Saud University – Science 33 (2021) 101252

Contents lists available at ScienceDirect

Journal of King Saud University – Science

journal homepage: www.sciencedirect.com

Original article

Nitrogen-doped carbon quantum dots (N-CQDs)/Co_3O_4 nanocomposite for high performance supercapacitor

Mu. Naushad [a,b,*], Tansir Ahamad [a], Mohd Ubaidullah [a,*], Jahangeer Ahmed [a], Ayman A. Ghafar [a], Khalid M. Al-Sheetan [a], Prabhakarn Arunachalam [c]

[a] Department of Chemistry, College of Science, King Saud University, 11451 Riyadh, Saudi Arabia
[b] Yonsei Frontier Lab, Yonsei University, Seoul, Korea
[c] Electrochemical Sciences Research Chair (ESRC), Chemistry Department, College of Science, P.O. Box 2455, King Saud University, Riyadh 11451, Saudi Arabia

ARTICLE INFO

Article history:
Received 8 October 2020
Revised 14 November 2020
Accepted 20 November 2020
Available online 3 December 2020

Keywords:
Hydrothermal route
Nitrogen doped carbon quantum dots
Metal oxide
Electrochemical studies
Energy storage and conversion

ABSTRACT

The search of low cost, highly competent electrode material is the hot research area for various next-gen applications. Herein, cost effective nitrogen doped carbon quantum dots (N-CQDs) anchored in cobalt oxide (Co_3O_4) nanocomposite was fabricated through a simple hydrothermal method. The fabricated N-CQDs/Co_3O_4 nanocomposite showed high specific surface area (BET) of ~880 $m^2\ g^{-1}$ with BJH pore size and volume of ~21 nm, 0.81945 $cm^3\ g^{-1}$ respectively. The electrochemical performance through cyclic voltammetry (CV) in 3-electrode systems exhibited an improved specific capacitance of 1782 F g^{-1} at 5 mV s^{-1} in 6 M KOH electrolyte. Additionally, galvanostatic charge–discharge (GCD) analysis showed an improved capacitive performance with a specific capacitance of 1867 F g^{-1} at 1 A g^{-1} current density. The energy density was calculated 36.9 Wh kg^{-1} at the power density of 480 W kg^{-1} The capacitance retention graph demonstrates 96% stability through 500 GCD cycles.

1. Introduction

The ever-increasing need of energy and depletion of fossil fuels is one of the main concerns across the globe. Clean renewable energy resources i.e. water, wind and solar needs the effective devices for storage, backup power and transportation of electricity (Cheng et al., 2012; Gao et al., 2015). The renewable energy equipment i.e. chemical energy can be converted into electrical energy through rechargeable batteries and reversible fuel cells (Cai et al., 2014). Electrochemical capacitors (ECs) also termed as supercapacitors (SCs) are immensely interesting potential energy storage devices owing to rapid charge–discharge high energy/power density with long life cycle (Ardizzone et al., 1990; Brousse et al., 2015; Xiong et al., 2020; Zheng et al., 1995). As per the charge storage mechanism, two main types of ECs are as follows; (1) the electrical double layer capacitors (EDLCs) works on electrostatic attraction amid ions and charged surfaces principle (Li et al., 2011; Wang et al., 2012). Electrode materials need to own exceptional electrical conductivity, exceptional BET surface area, porosity and chemical stability (Li et al., 2020). EDLCs are also known as traditional supercapacitors mainly based on a non-faradaic mechanism. The limited energy density of carbon EDLCs restricts their marketable applications in energy storage (Mukhiya et al., 2020; Yang et al., 2020). Moreover, pseudo capacitors own neither purely capacitive nor Faradaic processes (Shao et al., 2018) but in between EDLCs and batteries (Jiang and Liu, 2019; Srimuk et al., 2020). Numerous synthesis methods physical/chemical (Mironyuk et al., 2019; Shahat et al., 2015b, 2015a) and materials (metal oxide, sulphides, carbides, selenides etc.) have been checked among them transition MOs for instance; NiO (Al-Enizi et al., 2020) MnO_2 (Huang et al., 2015) and Co_3O_4 (Chen et al., 2020) show high theoretical capacitance i.e. 3560 F g^{-1} for Co_3O_4 than carbon based materials due to quick and reversible redox process and reckoned to be hopeful materials to increase the energy/power density of SCs. However, most reports show that the transition metal oxides' practical capacitances are less than theoretical values, due to relatively large particle size of TMOs nanoparticles (Suryanto et al., 2013). Moreover, carbon quantum dots are zero-dimensional nanomaterials having excellent chemical stability and functional-

* Corresponding authors: Department of Chemistry, College of Science, King Saud University, 11451 Riyadh, Saudi Arabia.
E-mail addresses: mnaushad@ksu.edu.sa (Mu. Naushad), mtayyab@ksu.edu.sa (M. Ubaidullah).
Peer review under responsibility of King Saud University.

Production and hosting by Elsevier

https://doi.org/10.1016/j.jksus.2020.101252
1018-3647/

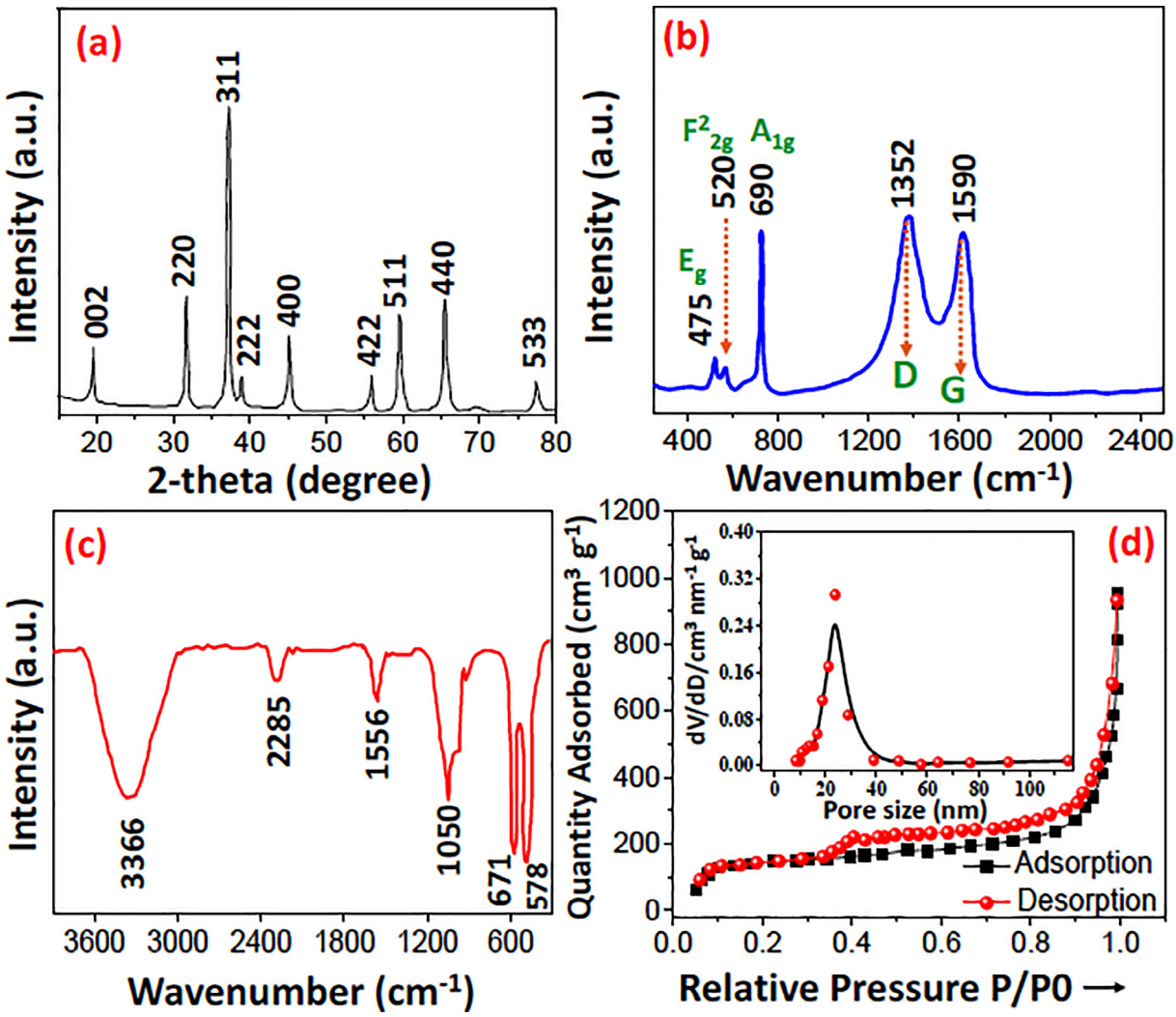

Fig. 1. (a) PXRD diffraction (b) Raman spectra (c) FTIR and (d) N_2 isotherm of N-CQDs/Co_3O_4 nanocomposite.

ization which enhance the electrochemical behaviour. In this report, we have fabricated a nanocomposite entailing of Nitrogen doped carbon quantum dots decorated in Co_3O_4 nanoparticles via a simple hydrothermal method. Co_3O_4 nanoparticles were synthesized as reported elsewhere (Fan et al., 2016). An excellent BET surface area was achieved which directly enhanced the electrochemical properties of N-CQDs/Co_3O_4 nanocomposite. The detailed description is given in the results and discussion section.

The fabrication of N-CQDs/Co_3O_4 nanocomposite was carried out in two steps.

2. Experimental

Chemicals used: Cobalt nitrate hexahydrate ($Co(NO_3)_2{\cdot}6H_2O$; Aldrich, 98% USA) sucrose ($C_{12}H_{22}O_{11,}$ ≥99.5 Aldrich, USA, melamine ($C_3H_6N_6$; Aldrich, USA), Polyvinylidene fluoride (CH_2CF_2n; Aldrich, USA) NMP (N-Methyl-2-pyrrolidone; Aldrich, USA) KOH (BDH; England), and utilized as received. Cobalt oxide (Co_3O_4) was prepared as per earlier reports via hydrothermal route (Fan et al., 2016).

2.1. Synthesis of nitrogen doped carbon quantum dost (N-CQDs)

To synthesize N-CQDs, melamine and sucrose were used as the source of Nitrogen and carbon respectively, 14 wt% (0.1130 g) of melamine ($C_3H_6N_6$) was added in 60 mL of DI H_2O and mixed through continuous stirring for 70 min. Subsequently, 1.5 g of sucrose was mixed to the previous transparent mixed solution at 55 °C with continuous stirring for 50 min. Later, this was poured to the Teflon autoclave reactor and heated at 170 °C for 6 hrs. Produced material was washed twice with help of ethanol/water and dried in vacuum at 65 °C for 5 hrs. Obtained powder referred to as N-CQDs.

2.2. Fabrication of N-CQDs/Co_3O_4 nanocomposite

In 100 mL of distilled water, 6 wt% of N-CQDs and 200 mg of Co_3O_4 nanoparticles were dispersed with the help of stirring for 45 min and ultrasonic treatment of 10 min. The obtained sample was centrifuged and dried at 50 °C for 15 hrs and further heated at 300 °C in Argon gas flow. A dark reddish black powder was obtained denoted as N-CQDs/Co_3O_4 nanocomposite. To characterize the N-CQDs/Co_3O_4 nanocomposite main analytical methods were used and elaborated in electronic supplementary information s-1. Additionally, electrochemical performance was checked on CHI-electrochemical work station by conducting cyclic volumetry (CV), galvanostatic charge–discharge (GCD), electrochemical impedance spectroscopy (EIS) tests in 6 M KOH with 3-electrode systems. The fabrication of working electrode detailed in S-2.

3. Results and discussion

3.1. Physicochemical Properties:

XRD analysis established the purity and phase of N-CQDs/Co_3O_4 nanocomposite as shown in Fig. 1a. The broad diffraction peaks at 2θ of 33.23°, 37.13°, 38.43°, 45.17°, 56.21°, 59.78°, 66.36° and 78.37° ascribed to 220, 311, 222, 400, 422, 511, 440 and 533 planes of cubic Co_3O_4 structure with JCPDS card no: 073-1701. The characteristic peak of carbon was indexed at 2θ of 19.38°, which certifies the presence of CQDs in the materials. The Raman spectra (Fig. 1b) showed two significant bands at 1352 and 1590 cm^{-1} belong to the D and G bands. The representative bands of Co_3O_4 at 475, 520 and 690 cm^{-1} ascribed to E_g, F^2_{2g} and A_{1g} modes, which confirms the formation of N-CQDs/Co_3O_4 nanocomposite. To assess the chemical bonds present in the materials, FTIR analysis was conducted, which distinctly verifies the existence of Cobalt-Nitrogen band at 578 cm^{-1} (Yuan et al., 2018). Moreover, the bands marked at 671, 1050, 1556, 2285 and 3366 cm^{-1} (Fig. 1c) ascribed to νC-N, νC-O-C, νCOO^-_{as} and broad band at 3366 cm^{-1} belongs to stretching vibrations of –OH bond due to the atmospheric moisture (Yang et al., 2020).

N_2 A-D isotherm (Fig. 1d) was conducted at 77 K in liquid Nitrogen. Moreover, the nitrogen adsorption desorption showed type IV isotherm with H2 hysteresis. Which shows the mono-multilayer adsorption. Excellent surface area (BET) of 880 $m^2\ g^{-1}$ with pore size and volume of 21 nm, 0.81945 $cm^3\ g^{-1}$ was analyzed in P/P_0 0.05–0.35 through multipoint BET equation (Al-Hartomy et al., 2013). The mesoporous nature of N-CQDs/Co_3O_4 nanocomposite was established by BJH pore size studies, which demonstrate a pore size of ~21 nm.

3.2. Structural elucidation

FE-SEM studies show the aggregated spherical particles with an average particle size ~28 nm as depicted in Fig. 2a.

Transmission electron microscopic studies (Fig. 2b) also validate the agglomeration of Co_3O_4 nanoparticles anchored with carbon quantum dots. The average particle size of N-CQDs/Co_3O_4 nanocomposite estimated to ~30 nm. HR-TEM analysis (Fig. 2c) displays the clear lattice fringes (Fig. 2c) with d-spacing of 0.280 nm, matching to 220 crystal planes of Co_3O_4 (cubic). Furthermore, Fig. 2d demonstrate the SAED patterns of CQDs/Co_3O_4 nanocomposite, indexed with 220, 311, 222, 400, 422, 511 and 440 planes from inward to outward direction which corroborated well with the XRD studies and confirmed the formation of N-CQDs/Co_3O_4 nanocomposite.

3.3. Electron spectroscopy for chemical analysis (ESCA or XPS)

The chemical composition/chemical state on the surface was estimated through XPS as shown in Fig. 3a–d. Fig. 3a demonstrate the survey spectrum of N-CQDs/Co_3O_4 nanocomposite consists of Carbon (C), Nitrogen (N), Oxygen (O) and Cobalt (Co) elements. Fig. 3b exhibits the HR- spectrum of Co2P shows 2 prime spin orbit peaks of $2P_{3/2}$, $2P_{1/2}$ at 781.18 eV, 597 eV and two satellite peaks. Moreover, the deconvolution of high-resolution spectrum of carbon peak (Fig. 3c) exhibits four peaks with the binding energy value 284.21, 285.28, 285.78 and ~288.07 eV, resembles to the C—C/C=C, C—N/C=N, C—O and C=O, respectively (Dou et al., 2016). HR-XPS of N exhibited in Fig. 3d as N1s, which is deconvoluted into 3 peaks with the binding energy of 398.24 eV, 400.14 eV and 401.46 eV corresponds to pyridinic-N, graphitic-N and

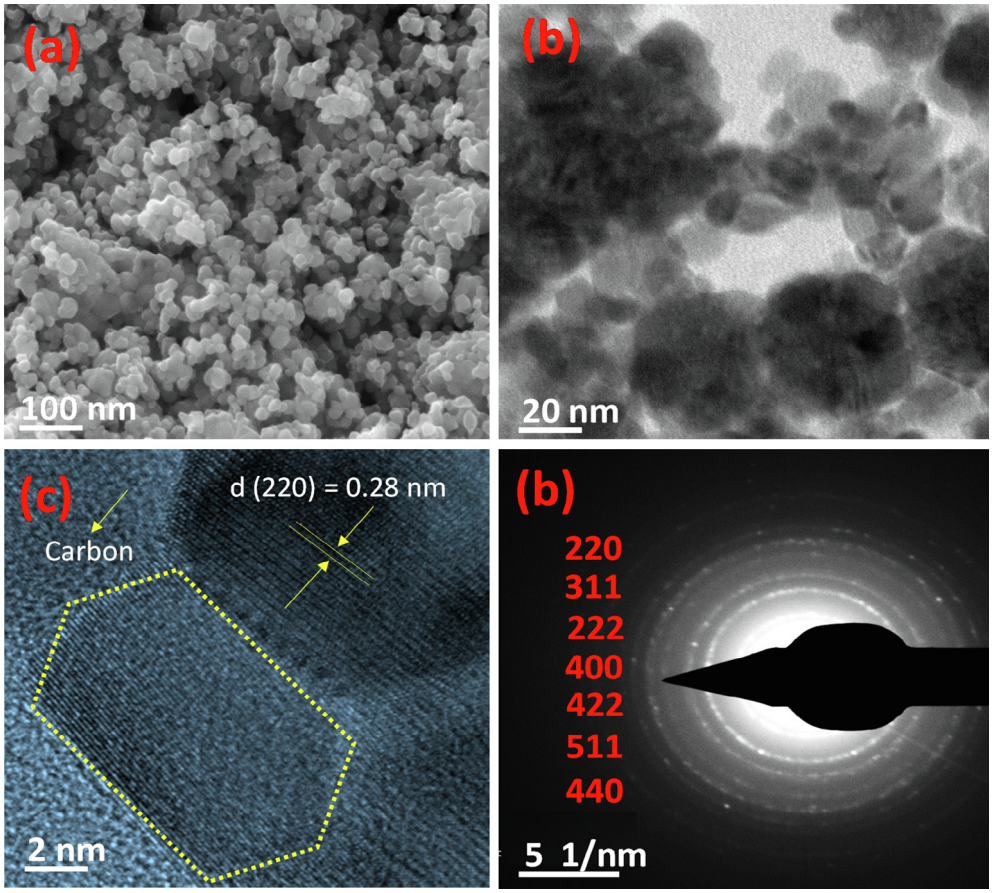

Fig. 2. (a) SEM micrograph (b) TEM micrograph (c) HR-TEM micrograph and (d) SAED patterns of N-CQDs/Co_3O_4 nanocomposite.

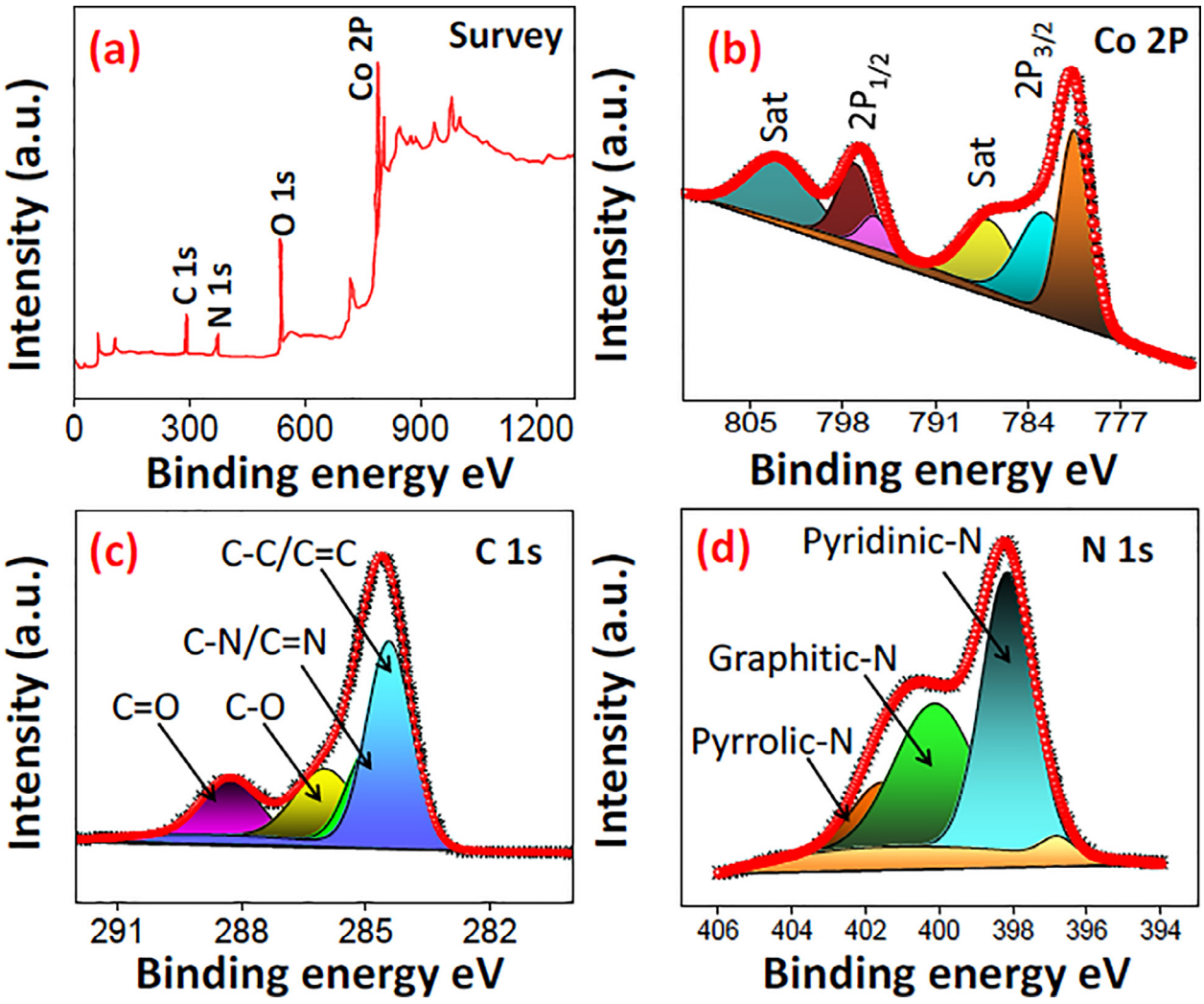

Fig. 3. XPS analysis of N-CQDs/Co3O4 nanocomposite. (a) survey spectrum (b) high resolution spectrum of Co 2P (c) high resolution spectrum of C1s and (d) high resolution spectrum of N1s.

pyrrolic-N (Alhokbany et al., 2020). The O 1s spectrum in S-3 exhibits the displays at 528.19, 531.15, and 535.18 eV, which belongs to Co—O, C—O, and O—H respectively. Such confirmation further endorses the formation of N-CQDs/Co_3O_4 nanocomposite

3.4. Electrochemical performance of N-CQDs/Co_3O_4 nanocomposite

The electrochemical behaviour of N-CQDs/Co_3O_4 nanocomposite were examined in a 3-electrode setup with 6 M KOH electrolyte through CV, GCD and EIS examination. CV experiments were conducted in a potential window of −0.4 to +0.6 V with scan rates starting from 5 mV s^{-1} to 100 mV s^{-1} as depicted in Fig. 4a. Apparent reduction–oxidation curves can be attributed to the reversible redox actions amid the changed valence states of cobalt. The electrochemical reaction mechanism is elaborated in S-4. The redox peaks of CV in Fig. 4a clearly indicate the charge storage mechanism is pseudocapacitive owing to Faradaic processes. An exceptional specific capacitance of 1782 F g^{-1} at 05 mV s^{-1} scan rate was recorded in 6 M KOH electrolyte. Moreover, galvanostatic charge–discharge (GCD) analysis revealed a better capacitive performance with a Cs of 1867 F g^{-1} at a current density of 1 A g^{-1}. The energy density was calculated 36.9 Wh kg^{-1} at the power density of 480 W kg^{-1} The capacitance retention graph exhibited 96% stability by examining upto 500 GCD cycles at a current density of 1 A g^{-1}. It is widely described that the carbon content can enhance the electrical conductivity and graphite N play an extremely vibrant part in supporting electron passage so that promotes the transportation of ions from electrolyte solution to interface (Karuppasamy et al., 2020).

To further explain the capacitance properties, the impedance studies of N-CQDs/Co_3O_4 nanocomposite in 100 kHz to 0.01 Hz was carried out at 5 mV. In Nyquist plot the high-frequency region a small semicircle supports the lower inner resistance and faster charge transfer at the electrode–electrolyte interface as shown Fig. 4f.

4. Conclusion

Cost effective mesoporous high specific surface area comprising N-CQDs/Co_3O_4 nanocomposite was fabricated through a simple hydrothermal route. High BET specific surface area of 880 m^2 g^{-1} and mesopores of 21 nm, with pore volume of 0.81945 cm^3 g^{-1}. The electrochemical performance through cyclic voltammetry (CV) in 3-electrode setup demonstrates an enhanced Cs of 1782 F g^{-1} at 05 mV s^{-1} in 06 M KOH electrolyte. Additionally, GCD studies demonstrate a better capacitive performance with a Cs of 1867

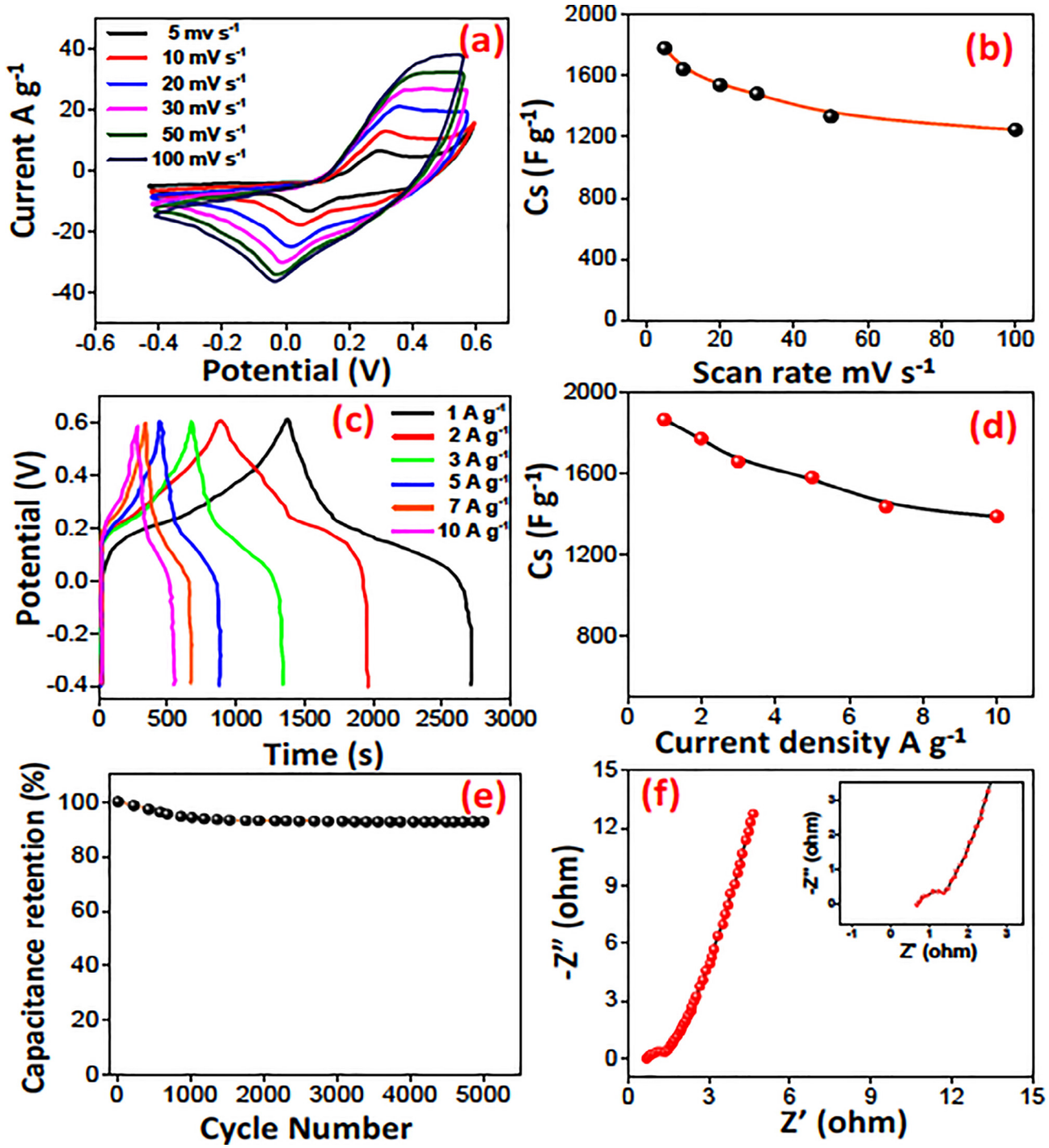

Fig. 4. Electrochemical analysis of N-CQDs/Co3O4 nanocomposite (a) cyclic voltammograms (b) Cs by CV (c) galvanostatic charge discharge curves (d) Cs by GCD (e) capacitance retention graph (f) Nyquist plot.

F g^{-1} at a current density of 1 A g^{-1}. The energy density was calculated 36.9 Wh kg^{-1} at the power density of 480 W kg^{-1} The capacitance retention graph revealed 96% stability by examining upto 500 GCD cycles. Excellent specific capacity of N-CQDs/Co_3O_4 nanocomposite electrode can be ascribed due to high specific BET surface area, and mesoporosity, which delivers profuse active sites for redox mechanism, and interconnected pores channels for the smooth passage of electrolyte ions and rapid reaction kinetics. Moreover, nitrogen doped graphitic carbon increase conductivity and better electron transport with the synergistic effect makes it a potential electrode materials for energy storage devices.

Declaration of Competing Interest

The authors declare that they have no known competing financial interests or personal relationships that could have appeared to influence the work reported in this paper.

Acknowledgement

The authors extend their appreciation to the Deputyship for Research & Innovation, "Ministry of Education" in Saudi Arabia

for funding this research work through the project number IFKSURG-1436-034.

Appendix A. Supplementary data

Supplementary data to this article can be found online at https://doi.org/10.1016/j.jksus.2020.101252.

References

Al-Enizi, A.M., Ubaidullah, M., Ahmed, J., Ahamad, T., Ahmad, T., Shaikh, S.F., Naushad, M., 2020. Synthesis of NiOx@NPC composite for high-performance supercapacitor via waste PET plastic-derived Ni-MOF. Compos. B Eng. 183, 107655. https://doi.org/10.1016/j.compositesb:2019.107655.

Al-Hartomy, O.A., Ubaidullah, M., Kumar, D., Madani, J.H., Ahmad, T., 2013. Dielectric properties of Ba1-xSrxZrO3 ($0 \leq x \leq 1$) nanoceramics developed by citrate precursor route. J. Mater. Res. 28 (8), 1070–1077. https://doi.org/10.1557/jmr.2013.40.

Alhokbany, N., Ahmed, J., Ubaidullah, M., Mutehri, S., Khan, M.A.M., Ahamad, T., Alshehri, S.M., 2020. Cost-effective synthesis of NiCo2O4@nitrogen-doped carbon nanocomposite using waste PET plastics for high-performance supercapacitor. J. Mater. Sci.: Mater. Electron. 31 (19), 16701–16707. https://doi.org/10.1007/s10854-020-04224-7.

Ardizzone, S., Fregonara, G., Trasatti, S., 1990. "Inner" and "outer" active surface of RuO2 electrodes. Electrochim. Acta 35 (1), 263–267. https://doi.org/10.1016/0013-4686(90)85068-X.

Brousse, T., Bélanger, D., Long, J.W., 2015. To be or not to be pseudocapacitive?. J. Electrochem. Soc. 162 (5), A5185–A5189. https://doi.org/10.1149/2.0201505jes.

Cai, Y., Wang, Y., Deng, S., Chen, G., Li, Q., Han, B., Han, R., Wang, Y., 2014. Graphene nanosheets-tungsten oxides composite for supercapacitor electrode. Ceram. Int. 40 (3), 4109–4116. https://doi.org/10.1016/j.ceramint.2013.08.065.

Chen, J., Xu, Z., Zhu, H., Liu, R., Song, X., Song, Q., Wu, J., Zhang, C., Ding, L., Dong, J., Cui, H., 2020. An ultrafast supercapacitor built by Co3O4 with tertiary hierarchical architecture. Vacuum 174, 109219. https://doi.org/10.1016/j.vacuum.2020.109219.

Cheng, Y., Lu, S., Zhang, H., Varanasi, C.V., Liu, J., 2012. Synergistic effects from graphene and carbon nanotubes enable flexible and robust electrodes for high-performance supercapacitors. Nano Lett. 12 (8), 4206–4211. https://doi.org/10.1021/nl301804c.

Dou, S., Li, X., Tao, L.i., Huo, J., Wang, S., 2016. Cobalt nanoparticle-embedded carbon nanotube/porous carbon hybrid derived from MOF-encapsulated Co 3 O 4 for oxygen electrocatalysis. Chem. Commun. 52 (62), 9727–9730. https://doi.org/10.1039/C6CC05244D.

Fan, H., Zhong, Y., Chang, L., Zhu, S., Wang, K., Shao, H., Wang, J., Zhang, J., Cao, C.-N., 2016a. Facile morphology controlled synthesis of nanostructured Co3O4 films on nickel foam and their pseudocapacitive performance. RSC Adv. 6 (58), 52957–52965. https://doi.org/10.1039/C6RA08117G.

Gao, G., Wu, H Bin, Ding, S., Liu, L.-M., Lou, X.W. (David), 2015. Hierarchical NiCo2O4 Nanosheets Grown on Ni Nanofoam as High-Performance Electrodes for Supercapacitors. Small 11, 804–808. https://doi.org/10.1002/smll.201402539.

Huang, M., Li, F., Dong, F., Zhang, Y.X., Zhang, L.L., 2015. MnO2 -based nanostructures for high-performance supercapacitors. J. Mater. Chem. A 3 (43), 21380–21423. https://doi.org/10.1039/C5TA05523G.

Jiang, Y., Liu, J., 2019. Definitions of pseudocapacitive materials: a brief review. Energy Environ. Mater. 2 (1), 30–37. https://doi.org/10.1002/eem2.12028.

Karuppasamy, K., Vikraman, D., Jeon, J.-H., Ramesh, S., Yadav, H.M., Rajendiran Jothi, V., Bose, R., Kim, H.S., Alfantazi, A., Kim, H.-S., 2020. Highly porous, hierarchical microglobules of Co3O4 embedded N-doped carbon matrix for high performance asymmetric supercapacitors. Appl. Surf. Sci. 529, 147147. https://doi.org/10.1016/j.apsusc.2020.147147.

Li, B., Cao, H., Shao, J., Li, G., Qu, M., Yin, G., 2011. Co3O4 @graphene composites as anode materials for high-performance lithium ion batteries. Inorg. Chem. 50 (5), 1628–1632. https://doi.org/10.1021/ic1023086.

Li, L., Dong, G., Xu, Y., Cheng, X., Gao, S., Zhang, X., Zhao, H., Huo, L., 2020. H3IDC-assisted synthesis of mesoporous ultrafine Co3O4/N-doped carbon nanowires as a high rate and long-life anode for Lithium-ion batteries. J. Alloys Compd 818, 152826. https://doi.org/10.1016/j.jallcom.2019.152826.

Mironyuk, I., Tatarchuk, T., Naushad, M., Vasylyeva, H., Mykytyn, I., 2019. Highly efficient adsorption of strontium ions by carbonated mesoporous TiO2. J. Mol. Liq. 285, 742–753. https://doi.org/10.1016/j.molliq.2019.04.111.

Mukhiya, T., Ojha, G.P., Dahal, B., Kim, T., Chhetri, K., Lee, M., Chae, S.-H., Muthurasu, A., Tiwari, A.P., Kim, H.Y., 2020. Designed assembly of porous cobalt oxide/carbon nanotentacles on electrospun hollow carbon nanofibers network for supercapacitor. ACS Appl. Energy Mater. 3 (4), 3435–3444. https://doi.org/10.1021/acsaem.9b02501.

Shahat, A., Awual, M.R., Khaleque, M.A., Alam, M.Z., Naushad, M., Chowdhury, A.M. S., 2015a. Large-pore diameter nano-adsorbent and its application for rapid lead (II) detection and removal from aqueous media. Chem. Eng. J. 273, 286–295. https://doi.org/10.1016/j.cej.2015.03.073.

Shahat, A., Awual, M.R., Naushad, M., 2015b. Functional ligand anchored nanomaterial based facial adsorbent for cobalt(II) detection and removal from water samples. Chem. Eng. J. 271, 155–163. https://doi.org/10.1016/j.cej.2015.02.097.

Shao, Y., El-Kady, M.F., Sun, J., Li, Y., Zhang, Q., Zhu, M., Wang, H., Dunn, B., Kaner, R. B., 2018. Design and mechanisms of asymmetric supercapacitors. Chem. Rev. 118 (18), 9233–9280. https://doi.org/10.1021/acs.chemrev.8b00252.

Srimuk, P., Su, X., Yoon, J., Aurbach, D., Presser, V., 2020. Charge-transfer materials for electrochemical water desalination, ion separation and the recovery of elements. Nat. Rev. Mater. 5 (7), 517–538. https://doi.org/10.1038/s41578-020-0193-1.

Suryanto, B.H.R., Lu, X., Zhao, C., 2013. Layer-by-layer assembly of transparent amorphous Co3O4 nanoparticles/graphene composite electrodes for sustained oxygen evolution reaction. J. Mater. Chem. A 1 (41), 12726. https://doi.org/10.1039/c3ta12672b.

Wang, G., Zhang, L., Zhang, J., 2012. A review of electrode materials for electrochemical supercapacitors. Chem. Soc. Rev. 41 (2), 797–828. https://doi.org/10.1039/C1CS15060J.

Xiong, S., Jiang, S., Wang, J., Lin, H., Lin, M., Weng, S., Liu, S., Jiao, Y., Xu, Y., Chen, J., 2020. A high-performance hybrid supercapacitor with NiO derived NiO@Ni-MOF composite electrodes. Electrochim. Acta 340, 135956. https://doi.org/10.1016/j.electacta.2020.135956.

Yang, J., Xu, X., Zhou, X., Jiang, S., Chen, W., Shi, S., Wang, D., Liu, Z., 2020. Ultrasmall Co3O4 nanoparticles confined in P, N-doped carbon matrices for high-performance supercapacitors. J. Phys. Chem. C 124 (17), 9225–9232. https://doi.org/10.1021/acs.jpcc.0c01539.

Yuan, M., Long, Y., Yang, J., Hu, X., Xu, D., Zhu, Y., Dong, Z., 2018. Biomass sucrose-derived cobalt@nitrogen-doped carbon for catalytic transfer hydrogenation of nitroarenes with formic acid. ChemSusChem 11 (23), 4156–4165. https://doi.org/10.1002/cssc.201802163.

Zheng, J.P., Cygan, P.J., Jow, T.R., 1995. Hydrous ruthenium oxide as an electrode material for electrochemical capacitors. J. Electrochem. Soc. 142 (8), 2699–2703. https://doi.org/10.1149/1.2050077.